



# Microbial activity and chemical weathering in the Middendorf aquifer, South Carolina

Jungho Park, Robert A. Sanford, Craig M. Bethke\*

Department of Geology, University of Illinois at Urbana-Champaign, 1301 West Green Street, Urbana, IL 61801, United States

## ARTICLE INFO

### Article history:

Received 3 June 2008

Received in revised form 9 October 2008

Accepted 10 October 2008

Editor: J. Fein

### Keywords:

Mineral alteration

Aquifer geochemistry

Groundwater microbiology

Sulfate reducing bacteria

Iron reducing bacteria

## ABSTRACT

We use reactive transport modeling to better understand the kinetics of chemical weathering in the Cretaceous Middendorf aquifer of South Carolina, USA, and the relationship of this process to subsurface microbial activity. We constructed a model accounting for the kinetics of mineral dissolution and precipitation, ion exchange, and the CO<sub>2</sub> and bicarbonate produced by iron reducing and sulfate reducing bacteria in the aquifer. We then fit the model to observed trends in the chemical composition of groundwater along the aquifer by adjusting the rate constants for the kinetic reactions considered. The modeling portrays weathering in the Middendorf as a slow process by which groundwater gradually reacts toward equilibrium with minerals in the aquifer. The rate constants predicted are 6 to 7 orders of magnitude smaller than measured in laboratory experiments and 3 to 4 orders of magnitude less than those inferred from weathering rates in soils. The rate constants are smaller even than expected by projecting observed trends with the duration of weathering to the geologic age of the Middendorf. Weathering is driven largely by biological activity: about half the acid consumed is CO<sub>2</sub> derived from the recharge area, and about half is supplied by iron reducing bacteria in the aquifer; only about 1% of the acid is of atmospheric origin, from CO<sub>2</sub> dissolved in rainwater.

© 2008 Elsevier B.V. All rights reserved.

## 1. Introduction

Geochemists are increasingly concerned with understanding the kinetics of chemical weathering, the degradation of minerals in the Earth's crust as it reacts with water and gases from the atmosphere and biosphere. Chemical weathering plays a critical role in the global geochemical cycle (Lasaga et al., 1994), the formation of supergene ores such as laterites (Soler and Lasaga, 1998), and the neutralization of acid rain (Drever and Hurcomb, 1986). Weathering rates are of intense current interest because of their relationship to the pace of global warming and shifts in the CO<sub>2</sub> balance over geologic time (Volk, 1987; Berner, 2006; Royer, 2006). Weathering creates soil and releases inorganic nutrients, such as sodium, calcium, potassium, magnesium, and phosphorus (Amundson, 2003). Deeper in the subsurface, the focus of this paper, understanding the rate of chemical weathering is critical to predicting the consequences of deep wastewater injection (Galloway, 1979), nuclear waste disposal (Fehrenbach et al., 1983), and CO<sub>2</sub> sequestration (Xu et al., 2005), as well as understanding the controls on groundwater chemistry and quality (Banks and Frengstad, 2006).

Chemical weathering is driven largely by reaction of minerals with meteoric water and acid gases, most notably CO<sub>2</sub>. Reaction consumes the acid, releasing cations to solution. CO<sub>2</sub> can be derived from the atmosphere and hence of an abiotic origin, and from biotic processes in the subsurface, such as root respiration and the oxidation of carbon

by microorganisms. Plants and microbes, then, can drive weathering directly, by generating CO<sub>2</sub>. Organisms can promote weathering in other ways, such as producing chelating agents, but those aspects of the problem are beyond the scope of this paper.

Most studies of the kinetics of chemical weathering have relied on laboratory experiments in which the analyst determines rate constants by observing how quickly minerals dissolve and precipitate. It has proven difficult to apply rate constants determined in this way to describe weathering rates in nature: the constants determined in the laboratory are as many as 5 orders of magnitude greater than those estimated from field studies of soils (Casey et al., 1993; Blum and Stillings, 1995; White and Brantley, 2003; Zhu, 2005). It is not clear, furthermore, how well rate constants determined by studying soils, which of course are geologically young, might describe weathering deeper in the subsurface, in much older aquifers.

Reaction rates measured in the laboratory decrease over time, as the initially fresh mineral surfaces age (White and Brantley, 2003), and the rates for geologically old minerals with undisturbed surfaces are likely to be quite small, too small to measure readily in the laboratory (Ganor et al., 2007). Reaction rates in natural soils, furthermore, decrease with the length of time the soil has been exposed to weathering, according to a power law (White and Brantley, 2003). The kinetics of weathering in the deeper subsurface, in the sediments and rocks below the soil zone, for these reasons, is poorly understood.

An alternative approach to quantifying weathering rates in the deeper subsurface is to infer reaction rates in an aquifer by direct study, from the chemical evolution of groundwater along a flow path (Kenoyer and Bowser, 1992; Rademacher et al., 2001; White, 2003;

\* Corresponding author. Tel.: +1 217 333 3369; fax: +1 217 244 4996.  
E-mail address: [bethke@illinois.edu](mailto:bethke@illinois.edu) (C.M. Bethke).

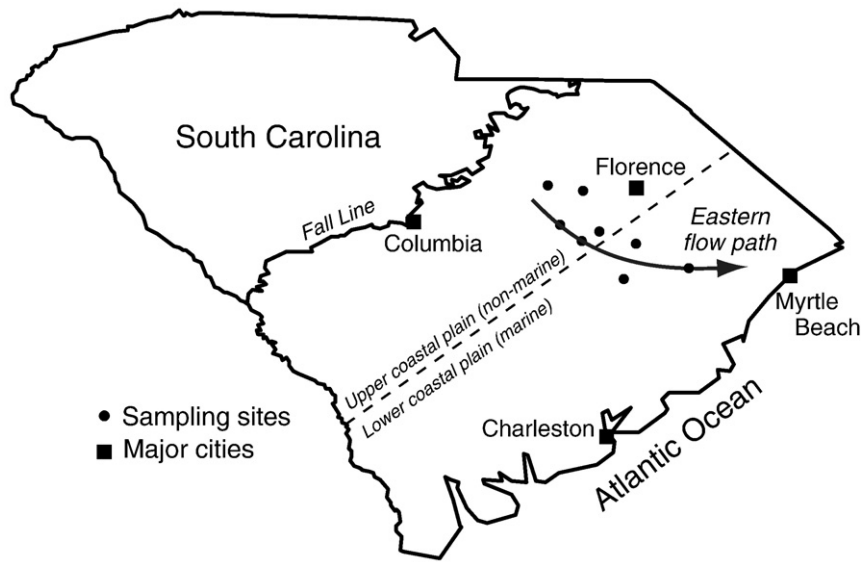


Fig. 1. Middendorf aquifer in South Carolina, showing approximate location of divide between upper and lower coastal plains (broken line), sampling sites (dots), and flow path considered in this study (Park et al., 2006).

Zhu, 2005; Banks and Frengstad, 2006; Hereford et al., 2007). In the studies cited, researchers observed differences in the chemical composition of groundwater between two points along a flow path. They then used a mass balance technique to estimate how much of various minerals dissolve and precipitate in the time required for groundwater to pass from one location to the other. Such inverse modeling, however, is not based on kinetic laws or thermodynamic principles and hence does not in itself yield values for the fundamental parameters describing weathering reactions.

In this paper, we use reactive transport modeling to determine directly the kinetic rate constants that describe chemical weathering in an ancient confined aquifer. Specifically, we construct a numerical model of groundwater flow, mass transport, and chemical reaction in the Cretaceous Middendorf aquifer of South Carolina, USA (Fig. 1). Fitting results of the model to trends in the chemical composition of groundwater observed along a flow path through the aquifer, we derive effective rate constants for mineral dissolution and precipitation reactions, and for ion exchange, applicable *in situ* over geologic time spans. Expressed mathematically, we use a reactive transport model to invert trends in the chemical composition of groundwater within the aquifer for the kinetic rate constants that describe reaction there. We then use the modeling to explore the relationship between chemical weathering and the production of CO<sub>2</sub> and bicarbonate by subsurface microbial populations.

2. Weathering and microbial activity

2.1. Middendorf aquifer

The Middendorf is a geochemically and microbiologically zoned aquifer within the Atlantic coastal plain (Fig. 1). The aquifer, which serves in South Carolina as a regional water supply, has been the subject of extensive scientific study (Aucott and Speiran, 1985; Chapelle and Lovley, 1990; McMahon and Chapelle, 1991; Chapelle and Lovley, 1992; Speiran and Aucott, 1994; Murphy and Schramke, 1998; Park et al., 2006). The clastic aquifer overlies crystalline bedrock and the sedimentary rocks of the Cape Fear formation (Fig. 2). It is exposed near the Fall Line and, to the southeast, covered by Cretaceous and Tertiary sedimentary rocks, reaching burial depths near the ocean of more than 1 km (Aucott and Roy, 1986). The aquifer contains detrital quartz and feldspar grains; kaolinite, illite, and smectite (Chapelle and Lovley, 1992; Speiran and Aucott, 1994); and, depending on the zone, ferric oxyhydroxide or carbonate detritus and cement.

Meteoric water saturated with oxygen recharges the aquifer along the Fall Line, where it is unconfined (Park et al., 2006). Groundwater velocity is relatively high here, up to about 20 m year<sup>-1</sup> (Sargent and Fliermans, 1989). Downgradient from the recharge area, in the confined section, groundwater is anaerobic. Water moves progressively more slowly along the direction of flow, as some of the flow is

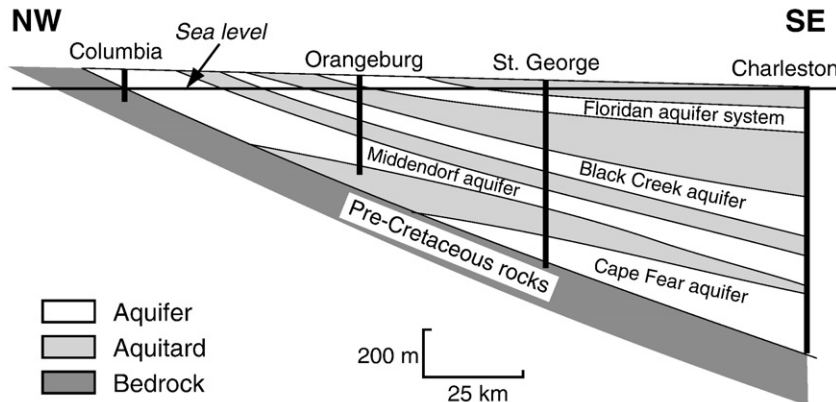


Fig. 2. Generalized geologic cross-section of the Middendorf aquifer from Columbia to Charleston (modified from Aucott and Speiran, 1985).

lost to discharge through the overlying confining units (Chapelle and Lovley, 1990). Groundwater in the confined portion of the aquifer flows at velocities of about 0.4 to 1 m year<sup>-1</sup> (Chapelle and Lovley, 1990).

In this paper, we consider microbial activity and chemical weathering along a flow path within the confined portion of the aquifer (Fig. 1). The flow path traverses much of the upper coastal plain, where iron reducing bacteria seem to predominate, and a section of the lower coastal plain immediately downstream, dominated by sulfate reducing bacteria. Since it takes hundreds of thousands of years for groundwater to traverse the study area, and since the aquifer is well sheltered from surface conditions by the confining layers, we assume the groundwater chemistry there remains stable over time, unaffected by seasonal change or climatic cycles.

Groundwater chemistry in the Middendorf varies across the flow path along trends shown by the symbols in Fig. 3, which represent chemical analyses from Park et al. (2006). The trends in chemistry along the direction of flow are the net result of microbial activity, mineral dissolution and precipitation reactions, and ion exchange (Park et al., 2006, and references therein). Our understanding of the importance and distribution of these reactions in the aquifer is derived largely from analysis of the chemical trends: from the rates at which species are added or removed, from the species' isotopic compositions, and from mineral saturation states calculated from species concentrations.

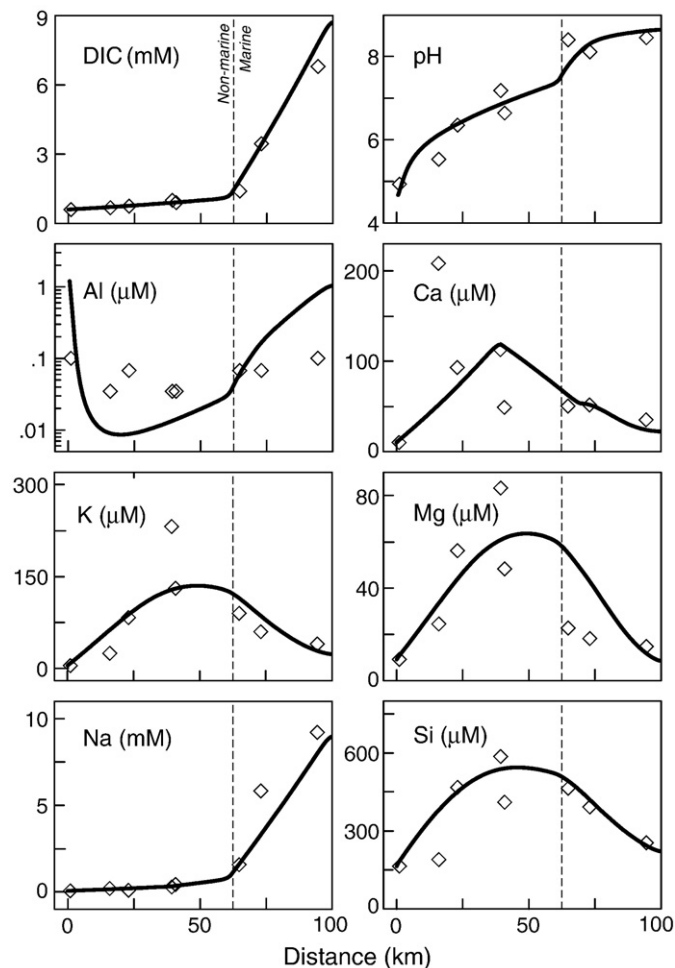


Fig. 3. Observed pH and chemical composition of groundwater from the Middendorf along the flow path (symbols; data from Park et al., 2006), and as predicted by the reactive transport model (solid lines, the results of this study), plotted against distance from the recharge area. DIC is dissolved inorganic carbon, CO<sub>2</sub> plus HCO<sub>3</sub>.

As is common in the study of freshwater aquifers, relatively little information is available on a regional scale about the petrology of the aquifer and its confining layers. There is, for example, no study of the distribution of quartz overgrowths or feldspar corrosion textures across the aquifer, which might provide an independent basis for estimating the rates of silica precipitation and feldspar dissolution in the subsurface. The remainder of this section describes current understanding of the distribution of microbial activity and weathering reactions within the aquifer, as treated in more detail by Park et al. (2006); in Section 3 we describe how we used this understanding to construct a reactive transport model.

## 2.2. Microbial activity

Microbial activity in the aquifer is supported by the breakdown of complex organic matter, represented here by the chemical formula C-H<sub>2</sub>O, within the fine-grained sediments of the sedimentary section (McMahon and Chapelle, 1991). Fermenting microorganisms degrade the organic matter into dihydrogen (H<sub>2</sub>), simple organic compounds such as acetate (CH<sub>3</sub>COO<sup>-</sup>) and formate (HCOO<sup>-</sup>), and carbon dioxide (CO<sub>2</sub>). The fermentation products migrate into the aquifer by diffusion or cross-formational flow, where the chemically reduced species are consumed by respiring microorganisms, primarily iron and sulfate reducers.

The net result of fermentation and respiration is the reduction of ferric iron and sulfate to form ferrous iron and sulfide, and the oxidation of the reduced carbon to produce CO<sub>2</sub> and bicarbonate (HCO<sub>3</sub><sup>-</sup>). Each of the microbiological zones in the aquifer is interpreted to result from the activity of a different functional group of microorganism (Lovley and Goodwin, 1988; Chapelle and Lovley, 1992). As described below, the distribution of the functional groups reflects depositional environment of the aquifer sediments (Speiran and Aucott, 1994).

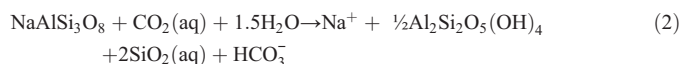
## 2.3. Upper coastal plain

In the upper coastal plain, the aquifer is composed of non-marine sediments rich in ferric oxyhydroxides (Chapelle and Lovley, 1992), represented here with the formula FeOOH, which are the products of weathering iron-bearing minerals under oxidized conditions. Groundwater here is generally soft, acidic, and low in dissolved solids. Once dissolved oxygen has been depleted, iron reducing bacteria appear to dominate microbial respiration. The iron reducers produce CO<sub>2</sub> and ferrous iron, driving up dissolved inorganic carbon (DIC; symbols in Fig. 3) and leaving the groundwater rich in iron. An overall reaction representing the fermentation of natural organic matter followed by iron reduction can be written



The reaction reflects the fact that although some of the iron stays in solution (Fe<sup>2+</sup> concentration in the upper coastal plain varies up to about 100 μM), much of it appears to precipitate, probably as a ferrous oxide component FeO(ox) within clay minerals (Park et al., 2006); this point is discussed further in Section 2.6.

By adding CO<sub>2</sub> to the groundwater, the iron reducers drive the weathering of aluminosilicate minerals. We can, for example, write a reaction by which albite (NaAlSi<sub>3</sub>O<sub>8</sub>) reacts with CO<sub>2</sub> to neutralize the acid (i.e., convert the CO<sub>2</sub> to bicarbonate, raising pH), precipitate kaolinite [Al<sub>2</sub>Si<sub>2</sub>O<sub>5</sub>(OH)<sub>4</sub>], and liberate silica:



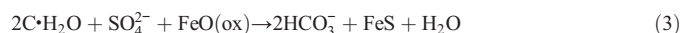
As a result of weathering reactions such as this, the concentrations of Na<sup>+</sup>, Mg<sup>2+</sup>, K<sup>+</sup>, Ca<sup>2+</sup>, and SiO<sub>2</sub>(aq) in the upper coastal plain increase along the direction of flow (Fig. 3). Groundwater pH increases here as

well (Fig. 3), reflecting the balance between the CO<sub>2</sub> produced by microbial activity and that consumed by weathering.

#### 2.4. Lower coastal plain

In the lower coastal plain, sediments lack ferric oxyhydroxides and sodium and bicarbonate ions make up the major portion of the dissolved load (Lee and Strickland, 1988). The depositional environment here is marine, the fine-grained sediments are richer in organic matter than in the upper coastal plain (Speiran and Aucott, 1994), and the DIC concentration increases along the direction of flow more rapidly (Fig. 3). The aquifer contains fine to medium-sized grains of detrital quartz and feldspar, sodium-rich marine clay minerals, abundant shell material, and calcite cement. Little or no ferric iron is available in the rock and the groundwater is low in iron, suggesting the absence of iron reduction. Instead, sulfate reducing bacteria, supported by the sulfate abundant in the marine section, appear to dominate microbial respiration.

The sulfate reducers consume the reduced fermentation products, along with sulfate, producing bicarbonate and sulfide. Sulfide does not accumulate in the groundwater, nowhere exceeding a concentration of 0.4 μM; instead, it likely reacts with ferrous iron in sediments to precipitate as iron sulfide (Park et al., 2006). An overall reaction representing fermentation followed by sulfate reduction can be written



There is little sulfate in the recharge, and sulfate along the aquifer, rather than being depleted, maintains a roughly constant concentration of about 100 μM (Park et al., 2006), about one-tenth the concentration of DIC. Given that sulfate-bearing minerals have not been identified within the Middendorf itself (Reid et al., 1986), sulfate to supply Reaction (3) must be transported into the aquifer from the confining layers, by diffusion or cross-formational flow (Chapelle and Lovley, 1990).

The sulfate supply may be derived from connate pore waters in the confining layers, from the dissolution of sulfate minerals there, or from ion exchange on fine-grained sediments. Sulfate ions, of course, cannot be added to the aquifer alone; they must be accompanied by counterions of positive charge. Consistent with the marine origin of sediments in the lower coastal plain, chemical trends in the aquifer (Fig. 3) indicate that Na<sup>+</sup> serves as the counterion, and for calculations in this paper we assume this is the case.

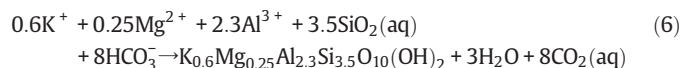
Groundwater chemistry in the lower coastal plain is further affected by the exchange on clay mineral surfaces of calcium for sodium ions



and, to a lesser extent, by calcite dissolution



(Speiran and Aucott, 1994). The net result of these reactions is an increase in the concentrations of Na<sup>+</sup> and HCO<sub>3</sub><sup>-</sup> in the water, and, since Reaction (4) dominates Reaction (5), a net loss of Ca<sup>2+</sup> (Fig. 3). Reaction (5) proceeds only slowly because, in the absence of iron reduction (Reaction (1)), there is no local source of CO<sub>2</sub> to drive it forward. The addition of bicarbonate serves to buffer pH to about 8.3, the midpoint pH between the CO<sub>2</sub>-HCO<sub>3</sub><sup>-</sup> and HCO<sub>3</sub><sup>-</sup>-CO<sub>3</sub><sup>2-</sup> buffers. Some aluminosilicate minerals dissolve in the lower coastal plain, as they do in the upper, but more slowly because they are more saturated, reflecting the higher pH and salinity. Other aluminosilicates such as illite are supersaturated and precipitate



decreasing the K<sup>+</sup> and Mg<sup>2+</sup> concentrations.

In contrast to iron reducers, sulfate reducers do not drive chemical weathering directly because, by Reaction (3), they produce bicarbonate rather than CO<sub>2</sub>. The sulfate reducers, nonetheless, promote weathering in the marine sediments because the bicarbonate serves to buffer the pH. By preventing pH from rising past a value of 8.3 as acid is consumed by weathering reactions, the buffering holds feldspars and calcite undersaturated, so they continue to dissolve.

#### 2.5. Respiration rates

The carbon isotopic composition of dissolved inorganic carbon in groundwater of the upper coastal plain indicates that the aqueous carbonate there is derived from the breakdown of organic matter (Chapelle and Lovley, 1992). The DIC increases 8 μM km<sup>-1</sup> along the flow path in the non-marine sediments (Park et al., 2006), reflecting the rate of microbial respiration. Taking groundwater velocity in the zone to be 0.6 m year<sup>-1</sup> and assuming a porosity of 20%, the DIC increase corresponds to a respiration rate of 3.0 × 10<sup>-20</sup> mol C cm<sup>-3</sup> s<sup>-1</sup> (expressed per cm<sup>3</sup> of aquifer, not fluid). Groundwater in the marine sediments of the lower coastal plain, in contrast, contains carbonate derived from not only organic decay but calcite dissolution (Chapelle and Lovley, 1992). The DIC increases 200 μM km<sup>-1</sup> along the flow path (Park et al., 2006) due to the combined effects of microbial activity and carbonate dissolution; the combined source rate, assuming velocity in the zone is 0.4 m year<sup>-1</sup>, is 5.3 × 10<sup>-19</sup> mol C cm<sup>-3</sup> s<sup>-1</sup>.

#### 2.6. Possibility of sulfate reduction in upper coastal plain

The high-iron groundwater found in the non-marine, ferric-rich sediments along the aquifer in upper coastal plain constitutes unambiguous evidence that iron reducing bacteria are active there (Chapelle and Lovley, 1992). Nonetheless, the iron concentrations observed can account for only a small fraction, nowhere more than 15%, of the microbial respiration occurring in the zone, as recorded by the increase in the DIC of the flowing groundwater (Park et al., 2006). A straightforward explanation of the shortfall in iron concentration, one that unless noted we assume in this paper to be correct, is that the majority of the Fe<sup>2+</sup> produced by the iron reducers is taken up as a minor component in clay minerals as they precipitate, as represented by Reaction (1).

An alternative explanation for some or all of the shortfall is that a certain but unknown fraction of the microbial respiration in the upper coastal plain is in fact due to bacterial sulfate reduction, rather than iron reduction. Sulfate reducers may even be the dominant group of microbes in the high-iron zone, because they generate a single H<sub>2</sub>S(aq) or HS<sup>-</sup> molecule for each pair of carbon atoms oxidized, whereas iron reducers produce eight Fe<sup>2+</sup> ions. If the aqueous sulfide and Fe<sup>2+</sup> react together to precipitate as FeS, for this reason, unreacted Fe<sup>2+</sup> may remain in solution, even where iron reduction is subordinate to sulfate reduction.

### 3. Reactive transport model

We constructed a reactive transport model of microbial activity and chemical weathering along a flow path (Fig. 1) through the Middendorf aquifer using program X1t from version 7.0.3 of The Geochemist's Workbench® Professional software package (Bethke, 2008), and the accompanying "thermo.dat" thermodynamic dataset (Delany and Lundeen, 1990). The input files used to run the model can be found in Appendix A of the online version of this paper. The model accounts for advection and dispersion of solutes in the flowing groundwater, the net effects of microbial activity, the rates at which various minerals precipitate and dissolve, and the kinetics of ion exchange in the aquifer. By fitting results of the model to the observed trends in pH and groundwater composition (Park et al., 2006), we determined a set of kinetic rate constants that describe chemical weathering in the aquifer.

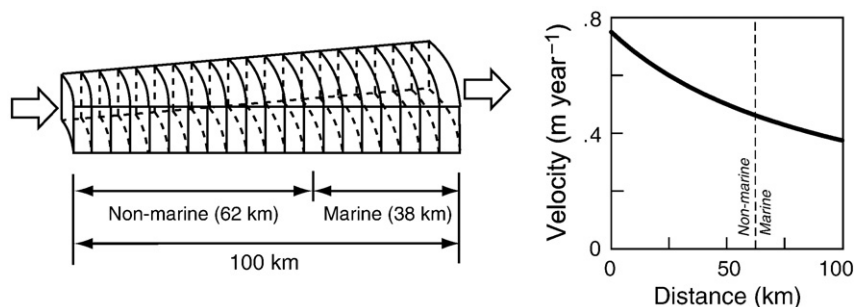


Fig. 4. Domain of reactive transport model (left), showing discretization used to obtain a numerical solution (the actual model contains 100 nodal blocks), and variation in groundwater velocity across the domain (right). Unreacted water enters the inlet at the left of the domain, displacing water from the outlet, at the right.

Our model differs conceptually from those employed in previous studies of the Middendorf. Speiran and Aucott (1994) developed a qualitative explanation of the relationship of pH and to DIC. Chapelle and Lovley (1990) applied the BALANCE software (Parkhurst et al., 1982) to estimate the rate of microbial carbonate production, using an inverse or mass balance approach. Murphy and Schramke (1998) developed a numerical model accounting for variation in isotopic composition using the NETPATH software, which also employs an inverse approach (Plummer et al., 1994). In contrast, we construct here a forward model that predicts variation in pH and chemical composition along the flow path on the basis of thermodynamic and kinetic laws.

### 3.1. Chemical and physical setting

The model tracks transport and reaction at 25 °C of the chemical components  $\text{Al}^{3+}$ ,  $\text{Ca}^{2+}$ ,  $\text{Cl}^-$  (which the model adjusts to achieve initial charge balance),  $\text{H}^+$  (to set pH),  $\text{HCO}_3^-$ ,  $\text{K}^+$ ,  $\text{Mg}^{2+}$ ,  $\text{Na}^+$ , and  $\text{SiO}_2(\text{aq})$ . The one-dimensional domain is 100 km long and, for purposes of obtaining a numerical solution, divided into 100 nodal blocks. To account for the gradual decrease in velocity along the flow path due to groundwater discharging to the surface (Speiran and Aucott, 1994), we configured the model in a diverging radial domain (Fig. 4). The leftmost 62 km of the domain is composed of non-marine sediments of the upper coastal plain, and the remaining 38 km are marine, lower coastal plain sediments.

Unreacted water enters from the left side of the domain, the inlet, displacing reacted water from the right, the outlet. We set groundwater velocity at the inlet to  $0.75 \text{ m year}^{-1}$  and sediment porosity across the domain to 20%. Owing to the radial geometry assumed, velocity decreases along the domain to a value of about  $0.38 \text{ m year}^{-1}$  by the time it reaches the outlet (Fig. 4). For comparison, a published estimate of the range of groundwater velocity in the confined portion of the Middendorf is 0.4 to  $1 \text{ m year}^{-1}$  (Chapelle and Lovley, 1990). Groundwater in the model takes about 200,000 years to traverse the domain. The diffusion coefficient in the model is  $10^{-6} \text{ cm}^2 \text{ s}^{-1}$  and longitudinal dispersivity is 10 m. Advective transport dominates diffusion and dispersion (the Péclet and grid Péclet numbers are large), and, as a result, the results are not sensitive to variation in the choice of diffusion coefficient or dispersivity, nor the number of nodal blocks used.

Flow in the aquifer has been stable over millions of years, so we determined the steady state solution by running the model forward from arbitrary initial conditions until the fluid had been displaced 10 times, well past the point at which groundwater composition and the distribution of reactions within the domain stabilized. We used the composition of groundwater in the recharge area (Table 1; Park et al., 2006) as the inlet boundary condition. We took the same water composition as the initial condition for the simulation, which as we noted is arbitrary, except we increased the  $\text{Ca}^{2+}$  concentration (and hence the concentration of  $\text{Cl}^-$ , the charge balance ion in the model) by

a factor of five. This setting prevents the ion exchange reaction with  $\text{Na}^+$  from being so far from equilibrium that it inhibited the model from time marching, the procedure it uses to advance from the initial condition toward the long-term result we seek; since the initial conditions are arbitrary, the  $\text{Ca}^{2+}$  concentration chosen does not affect the steady-state solution.

### 3.2. Microbial activity

We assume, except where noted, that microbial activity is dominated in the upper coastal plain by fermentation of natural organic matter followed by iron reduction, and in the lower coastal plain by fermentation and then sulfate reduction. Unlike the weathering reactions, which proceed in the model at rates predicted by kinetic rate laws, as described next (Section 3.3), the rates of iron reduction and sulfate reduction in the calculation are prescribed directly as constraints on the calculation, because the rates of microbial respiration in the aquifer are known (Section 2.5).

Iron reduction affects groundwater chemistry in the model by contributing one mole of  $\text{CO}_2$  for each mole of  $\text{C-H}_2\text{O}$  fermented, by Reaction (1). Since we specify the rate this reaction proceeds in advance, and because iron takes no part in the weathering reactions considered (Section 3.3), we need not include explicitly in the model the transport and reaction of iron species. The sulfate reducers, according to Reaction (3), generate a mole of  $\text{HCO}_3^-$  per mole of  $\text{C-H}_2\text{O}$  consumed. Sulfate reduction has the further effect of adding a mole of  $\text{Na}^+$  to groundwater in the aquifer per mole of  $\text{C-H}_2\text{O}$  fermented, because, as previously discussed (Section 2.4), the supply to the aquifer of the sulfate ions to be consumed by Reaction (3) is charge balanced by the addition of sodium ions. Again, since the rate of sulfate reduction is set directly and sulfur plays no part in the weathering reactions considered, we do not explicitly include sulfur species in the calculation.

### 3.3. Weathering reactions

Each of the minerals shown in Table 2 reacts in the model according to a kinetic rate law, at a rate  $r$  ( $\text{mol cm}^{-3} \text{ s}^{-1}$ ), expressed per

Table 1  
Composition of inlet water

pH	4.5
$\text{Al}^{3+}$	0.1 $\mu\text{M}$
$\text{Ca}^{2+}$	10 $\mu\text{M}$
$\text{Cl}^-$	125 $\mu\text{M}$
$\text{CO}_2(\text{aq})$	600 $\mu\text{M}$
$\text{K}^+$	4.4 $\mu\text{M}$
$\text{Mg}^{2+}$	9.2 $\mu\text{M}$
$\text{Na}^+$	58 $\mu\text{M}$
$\text{SiO}_2(\text{aq})$	160 $\mu\text{M}$

**Table 2**  
Kinetic reactions considered in reactive transport model

Mineral	Kinetic reaction	log <i>K</i> <sup>a</sup>
Albite	NaAlSi <sub>3</sub> O <sub>8</sub> + 4H <sup>+</sup> → Na <sup>+</sup> + Al <sup>3+</sup> + 3SiO <sub>2</sub> (aq) + 2H <sub>2</sub> O	3.097
Anorthite	CaAl <sub>2</sub> Si <sub>2</sub> O <sub>8</sub> + 8H <sup>+</sup> → Ca <sup>2+</sup> + 2Al <sup>3+</sup> + 2SiO <sub>2</sub> (aq) + 4H <sub>2</sub> O	27.06
Illite	K <sub>0.6</sub> Mg <sub>0.25</sub> Al <sub>2.3</sub> Si <sub>3.5</sub> O <sub>10</sub> (OH) <sub>2</sub> + 8H <sup>+</sup> → 0.6K <sup>+</sup> + 0.25Mg <sup>2+</sup> + 2.3Al <sup>3+</sup> + 3.5SiO <sub>2</sub> (aq) + 5H <sub>2</sub> O	9.804
Kaolinite	Al <sub>2</sub> Si <sub>2</sub> O <sub>5</sub> (OH) <sub>4</sub> + 6H <sup>+</sup> → 2Al <sup>3+</sup> + 2SiO <sub>2</sub> (aq) + 5H <sub>2</sub> O	7.430
Quartz	SiO <sub>2</sub> → SiO <sub>2</sub> (aq)	-3.999
Calcite	CaCO <sub>3</sub> + H <sup>+</sup> → Ca <sup>2+</sup> + HCO <sub>3</sub> <sup>-</sup>	1.713
Dolomite	CaMg(CO <sub>3</sub> ) <sub>2</sub> + 2H <sup>+</sup> → Ca <sup>2+</sup> + Mg <sup>2+</sup> + 2HCO <sub>3</sub> <sup>-</sup>	2.521
Ion exchange	Na <sub>2</sub> -clay + Ca <sup>2+</sup> → Ca-clay + 2Na <sup>+</sup>	0.796

<sup>a</sup> At 25 °C, from Delany and Lundeen (1990), Appelo and Postma (1993).

cm<sup>3</sup> of the aquifer) that is positive for dissolution and negative for precipitation. Over the pH range of interest (approximately 5 to 8), reaction of the minerals considered is described by the rate law

$$r = k \left( 1 - \frac{Q}{K} \right) \quad (7)$$

where *Q* and *K* are the activity product and equilibrium constant for the dissolution reaction (Soler and Lasaga, 1998). Here, *k* is the effective rate constant (mol cm<sup>-3</sup> s<sup>-1</sup>), given by

$$k = V\rho A_s k_+ \quad (8)$$

where *V* is the volume fraction in the aquifer of the mineral in question,  $\rho$  is the mineral's density (g cm<sup>-3</sup>), *A<sub>s</sub>* is its specific surface area (cm<sup>2</sup> g<sup>-1</sup>), and *k<sub>+</sub>* is the intrinsic kinetic rate constant (mol cm<sup>-2</sup> s<sup>-1</sup>) for the reaction.

We assume the effective rate constants for the mineral reactions are invariant across the domain, except for calcite and dolomite, which are not present in the upper coastal plain and hence are not allowed to react there. We allow dolomite to precipitate in the model, although this reaction may be a proxy for the precipitation of a magnesian component within the calcite. It is not well known whether, over the hundreds of thousands of years groundwater is resident in the aquifer, dolomite can form, either by abiotic means or through microbial mediation (e.g., Roberts et al., 2004). Similarly, given the long residence time of water in the aquifer, we take quartz as the sink for silica, although in reality an unknown fraction of the silica may precipitate to form faster reacting phases, such as opal.

### 3.4. Ion exchange

Ion-exchange (Reaction (4)), which occurs mainly in the marine sediments, is allowed to proceed in the rightmost 60 km. We assume the reaction proceeds as a kinetic process, at a rate given by Eq. (7). The ion activity product *Q* for the reaction is given

$$Q = \frac{[\text{Ca-clay}][\text{Na}^+]^2}{[\text{Na}_2\text{-clay}][\text{Ca}^{2+}]} \quad (9)$$

where the brackets represent activity. By assuming the exchangeable components Ca-clay and Na<sub>2</sub>-clay in the marine sediments are in equilibrium with sea water, we calculated the ratio [Ca-clay]/[Na<sub>2</sub>-clay] from the concentrations of Na<sup>+</sup> and Ca<sup>2+</sup> in seawater and an equilibrium constant *K* of 6.25 for Ca-Na exchange cited by Appelo and Postma (1993). The ion activity product can then be represented

$$Q = 0.3 \times \frac{[\text{Na}^+]^2}{[\text{Ca}^{2+}]} \quad (10)$$

from the calculated ratio of 0.3.

### 3.5. Modeling procedure

We determined the effective kinetic rate constants for the mineral dissolution and precipitation reactions, and for ion exchange, by fitting the reactive transport model to the trends in groundwater composition observed in the aquifer, according to the following procedure:

1. Set rates of iron reduction in the non-marine sediments, and sulfate reduction in the marine sediments to values that reproduce the trends in DIC composition in the upper and lower coastal plains. The rate for sulfate reduction is set tentatively at this point, because the rate of calcite dissolution is not known.
2. Set the effective rate constant for illite dissolution and precipitation to a value that reproduces the data for K<sup>+</sup> and Mg<sup>2+</sup>.
3. Set the effective rate constants for the dissolution of albite and anorthite to reproduce the trends for Na<sup>+</sup> and Ca<sup>2+</sup> in the upper coastal plain.
4. Set the effective rate constant for ion exchange to simulate the pattern of Na<sup>+</sup> increase and Ca<sup>2+</sup> decrease in the rightmost 60 km of the domain.
5. Set the effective rate constant for kaolinite precipitation to give Al<sup>3+</sup> concentrations bracketing those measured.
6. Set the effective rate constant of quartz precipitation to a value simulating the trends in SiO<sub>2</sub>(aq) concentration.
7. Set the effective rate constant of calcite dissolution to reflect Ca<sup>2+</sup> concentrations in the lower coastal plain.
8. Set the effective rate constant of dolomite precipitation to simulate Mg<sup>2+</sup> concentrations in the lower coastal plain.
9. Adjust the rate of sulfate reduction in the lower coastal plain to improve the fit to DIC in the lower coastal plain.
10. Repeat steps (2) through (9) until the fit to the observed data no longer improves.

## 4. Results

Following the procedure outlined in the previous section, we fit the reactive transport model to the trends in pH and groundwater composition observed in the aquifer, using the effective rate constants shown in Table 3; Fig. 3 shows the model results. We were able to reproduce the general trends in most of the data and made no attempt to match individual data points. The exception is the trend for Al<sup>3+</sup>, for which the model results correspond poorly to observation. Aluminum analyses of natural waters are commonly affected by colloids and fine sediments which pass through the filter during sampling, and a poor correspondence between theoretical calculations and field observations is commonly noted for this minor element. Fig. 5 shows saturation indices (log *Q*/*K*) for minerals predicted by the model compared to those calculated from the chemical analyses, along with log *Q*/*K* values predicted for the ion exchange reaction. The saturation indices calculated for illite and kaolinite are imprecise, being affected not only by the error inherent in analyzing for aluminum, but by

**Table 3**  
Effective kinetic rate constants *k* (mol cm<sup>-3</sup> s<sup>-1</sup>) used in reactive transport model

Reaction	Rate constant	Interval (km) <sup>a</sup>
Albite	2.60 × 10 <sup>-20</sup>	
Anorthite	1.15 × 10 <sup>-20</sup>	
Illite	2.80 × 10 <sup>-20</sup>	
Kaolinite	0.70 × 10 <sup>-20</sup>	
Quartz	1.20 × 10 <sup>-20</sup>	
Calcite	1.00 × 10 <sup>-20</sup>	70–100
Dolomite	0.50 × 10 <sup>-21</sup>	70–100
Ion exchange	1.85 × 10 <sup>-20</sup>	40–100

<sup>a</sup> Reaction applies across domain, unless noted.

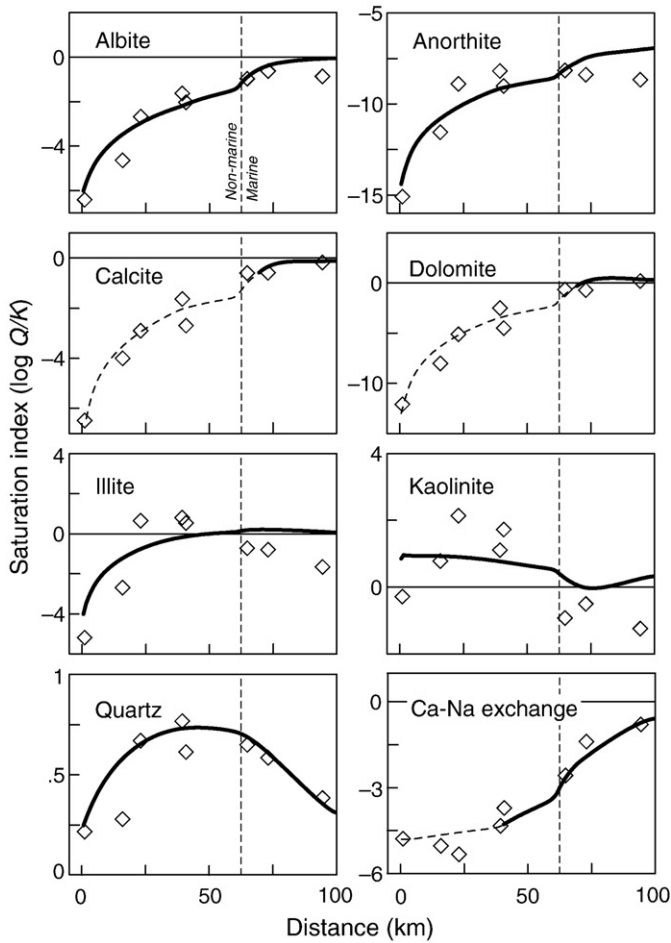
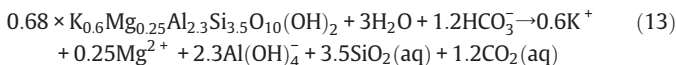
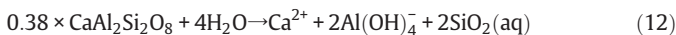


**Fig. 5.** Saturation indices ( $\log Q/K$ ) of minerals predicted by the reactive transport model (solid lines; broken lines where reaction in question is not considered), and calculated from observed groundwater composition (symbols). Negative saturation indices represent undersaturation; positive, supersaturation. Plot also shows  $\log Q/K$  for the ion exchange reaction. Calculated indices for the aluminosilicates, especially illite and kaolinite, are affected rather strongly not only by uncertainty in the minerals' stabilities, but by uncertainty in determining aluminum concentration in the groundwater, as discussed in text, and hence carry broad error ranges (not shown).

uncertainty in the minerals' stabilities, and hence scatter about the trends shown in Fig. 5. Fig. 6 shows the reaction rates predicted for mineral dissolution and precipitation in the aquifer, and for ion exchange.

#### 4.1. Upper coastal plain

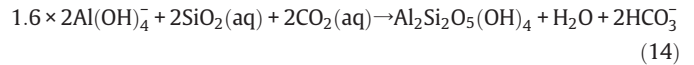
In the non-marine sediments of the upper coastal plain, albite, anorthite and illite are everywhere, or almost everywhere, undersaturated in the model results. The minerals dissolve, consuming acid and hence raising pH, and driving up the concentrations of  $\text{Na}^+$ ,  $\text{Ca}^{2+}$ ,  $\text{K}^+$ ,  $\text{Mg}^{2+}$ , and  $\text{SiO}_2(\text{aq})$  in the groundwater. Normalized to the rate at which iron reduction produces  $\text{CO}_2$  ( $3.0 \times 10^{-20} \text{ mol C cm}^{-3} \text{ s}^{-1}$ ), the minerals at an arbitrary point 25 km from the recharge area dissolve according to



For each mole of  $\text{CO}_2$  produced by the iron reducers at this point in the aquifer, for example, 0.85 mol of albite dissolves, contributing to solution 0.85 mol of sodium and alumina, and  $3 \times 0.85 = 2.55$  mol of

silica. The absolute rate of albite dissolution is  $0.85 \times 3.0 \times 10^{-20} \text{ mol cm}^{-3} \text{ s}^{-1} = 2.55 \times 10^{-20} \text{ mol cm}^{-3} \text{ s}^{-1}$ , and so on for the other reactions.

In response to the alumina and silica liberated by these reactions, kaolinite and quartz precipitate in the model according to



For each mole of acid contributed by iron reduction, weathering by Reactions (11–15) consumes an additional 1.4 mol of acid as  $\text{CO}_2$  from the recharge. Taking the reactions together, weathering liberates per mole of iron reduction a total of 0.85 mol of  $\text{Na}^+$ , 0.38 mol of  $\text{Ca}^{2+}$ , 0.41 mol of  $\text{K}^+$ , 0.17 mol of  $\text{Mg}^{2+}$ , 1.0 mol of  $\text{SiO}_2(\text{aq})$ , and 2.4 mol of  $\text{HCO}_3^-$ . The iron reducing bacteria, then, account for about 40% of the acid that drives the chemical weathering of aluminosilicates at this point in the upper coastal plain.

#### 4.2. Lower coastal plain

In the marine sediments of the lower coastal plain, albite dissolves, but more slowly than in the upper plain, because pH is higher (Fig. 3) and hence the mineral is less undersaturated (Fig. 5). Anorthite, in contrast, is sufficiently undersaturated in the simulation (Fig. 5) that across the flow line the  $(1 - Q/K)$  term in Eq. (7) remains close to unity, rendering the dissolution rate invariant.  $\text{Ca}^{2+}$  in the water exchanges with  $\text{Na}^+$  (Reaction 4), calcite dissolves, and kaolinite, illite, quartz, and dolomite precipitate. The  $\text{HCO}_3^-$  generated by sulfate reduction

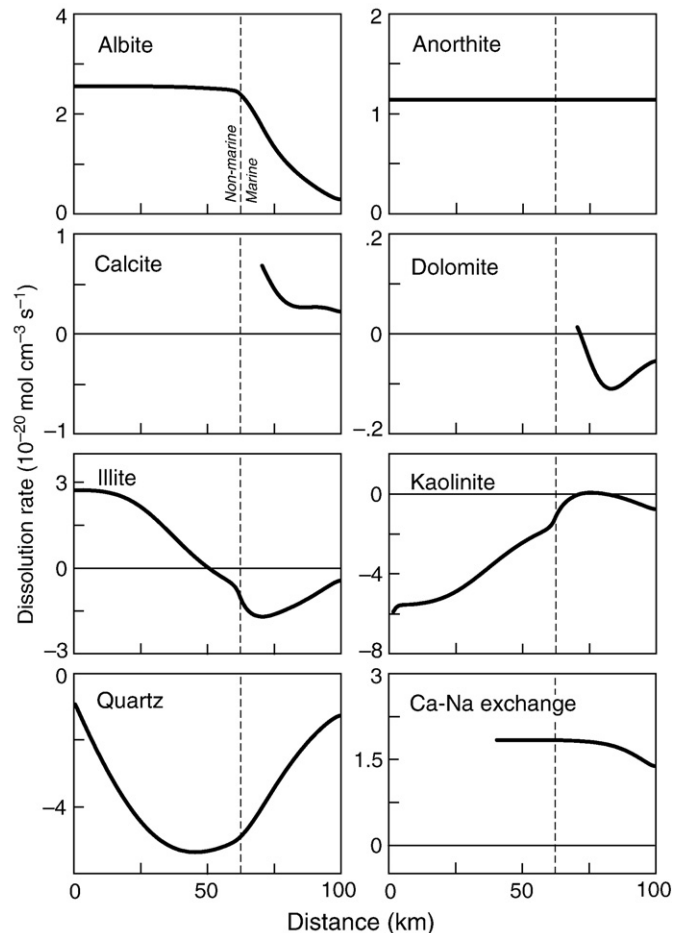
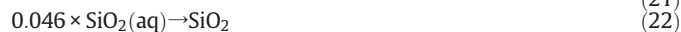
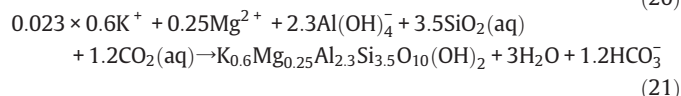
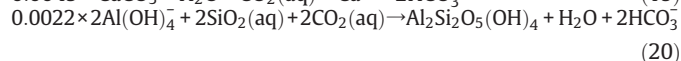
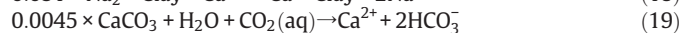
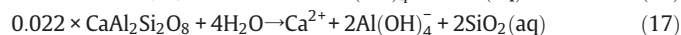
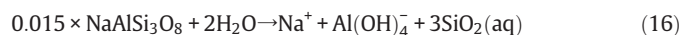


**Fig. 6.** Reaction rates ( $\text{mol cm}^{-3} \text{ s}^{-1}$ ) in reactive transport model. For minerals, positive values represent dissolution and negative values, precipitation.

(Reaction 3) helps buffer pH to a value near 8.3, as already discussed (Section 2.4).

Normalized to the rate at which sulfate reduction produces  $\text{HCO}_3^-$  ( $5.3 \times 10^{-19} \text{ mol C cm}^{-3} \text{ s}^{-1}$ ), the reactions occurring at a point 85 km from the recharge area are



Taken together, the reactions consume 0.033 mol of acid as  $\text{CO}_2$ , 0.043 mol of  $\text{SiO}_2(\text{aq})$ , 0.0070 mol of  $\text{Ca}^{2+}$ , 0.014 mol of  $\text{K}^+$ , and 0.0079 mol of  $\text{Mg}^{2+}$ , and produce 1.1 mol of  $\text{Na}^+$  and 1.03 mol of  $\text{HCO}_3^-$ . From the small normalized rate of 0.0045 for Reaction (19), we see that at this location in the model sulfate reduction, rather than calcite dissolution, is the principal source to the flowing groundwater of DIC.

## 5. Discussion

### 5.1. Intrinsic rate constants

The intrinsic rate constants suggested by this study are considerably smaller than those obtained by laboratory experiment, or by study of reaction in soils, even accounting for the known tendency of the rate constants to decrease with the duration of weathering. Table 4 shows intrinsic rate constants for quartz, albite, and kaolinite estimated using Eq. (8) from the effective rate constants derived in this study (Table 3). For comparison, Table 4 also shows intrinsic rate constants for the minerals derived from laboratory and field study. Lacking precise knowledge of the aquifer's composition, we assume the minerals make up, respectively, 50%, 10%, and 5% of the Middendorf. Following convention in geochemistry, we use in the calculation specific surface areas measured in the laboratory with the BET method (Berger et al., 1994; White et al., 1996). By this convention, a small rate constant predicted for a mineral in the aquifer might reflect not only the mineral being in an unreactive state, but occlusion in the aquifer of the mineral's surface area. The effect of a diminution in a mineral's surface area, in other words, cannot be distinguished here from chemical effects normally associated with the intrinsic rate constant, such as variation in the mineral's reactivity as its surface ages and anneals.

**Table 4**  
Comparison of intrinsic rate constants  $k_r$  ( $\text{mol cm}^{-2} \text{ s}^{-1}$ )

	Rate constant from laboratory measurement <sup>a</sup>	Rate constant from soil profiles <sup>b</sup>	Specific surface area ( $\text{cm}^2 \text{ g}^{-1}$ ) <sup>c</sup>	Rate constant from this study <sup>d</sup>
Quartz	$4.2 \times 10^{-18}$	$1.1 \times 10^{-19}$	$1.5 \times 10^3$	$6.0 \times 10^{-24}$
Albite	$5.5 \times 10^{-17}$	$1.0\text{--}1.3 \times 10^{-20}$	$1.4 \times 10^4$	$7.1 \times 10^{-24}$
Kaolinite	$5.0 \times 10^{-18}$		$11.2 \times 10^4$	$4.8 \times 10^{-25}$

<sup>a</sup> Laboratory measurement by Soler and Lasaga (1998).

<sup>b</sup> Estimated for soil profiles using measured BET surface areas (White et al., 1996; Schulz and White, 1999; Zhu, 2005).

<sup>c</sup> Laboratory measurement (Carroll-Webb and Walther, 1988; Berger et al., 1994; White et al., 1996).

<sup>d</sup> Calculated by Eq. (8) from the effective rate constants (Table 3) and specific surface areas shown. The densities of quartz, albite, and kaolinite are  $2.648 \text{ g cm}^{-3}$ ,  $2.616 \text{ g cm}^{-3}$ , and  $2.594 \text{ g cm}^{-3}$ , respectively, and the minerals are assumed to make up 50%, 10%, and 5% of the aquifer.

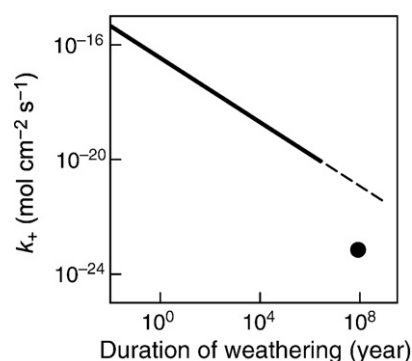


**Fig. 7.** Intrinsic rate constant for albite dissolution obtained in this study (circle), compared to trend in the rate constant with the duration of weathering (line), as observed for plagioclase in soils by White and Brantley (2003). Line is broken where trend is extrapolated beyond 3 m.y.

The intrinsic rate constants predicted for the Middendorf are about 6 to 7 orders of magnitude smaller than those measured in the laboratory, and about 3 to 4 orders of magnitude less than those observed for weathering in soils (Table 4). The principal uncertainty in estimating effective rate constants by reactive transport modeling, as we have done in this study, is commonly the choice of groundwater velocity, because the rate constants derived scale directly with the value assumed for this variable. The discrepancies noted among rate constants are much too large to be explained by an imprecise estimate of velocity, which is almost certainly known to within a factor of a single order of magnitude.

Fig. 7 shows the value of the rate constant for albite from this study, compared to a power law showing how rate constants for plagioclase feldspar in soils decrease with the duration of weathering (White and Brantley, 2003).<sup>1</sup> The power law is based on weathering ages of up to 3 m.y., but if we extend it to the geologic age of the Middendorf, about 80 m.y., we see it passes about two orders of magnitude above the value for albite. The rate constant predicted for the ancient Middendorf sediments, then, is smaller by about a hundred-fold than might be expected by extrapolating the trends observed in geologically young soils.

The rate constants representing weathering in the Middendorf probably take on small values for a number of reasons. The reactivity of mineral surfaces decreases with time, as the most reactive spots such as steps and defects on the surface dissolve. Reactive surfaces can become coated with secondary minerals, as a result of incongruent dissolution. And the surfaces can be occluded by sedimentary cements, organic matter, and contact with other minerals (Velbel, 1993; Nugent et al., 1998; White and Brantley, 2003). Soils are more biologically active than deep aquifers, furthermore, and weathering there may be enhanced organically by the production of chelating agents (Hiebert and Bennett, 1992; Bennett et al., 1996; Welch and Ullman, 1999). Large differences in the rate constants between soils and the Middendorf are less likely to arise from thermodynamic effects, or the effect of variations in pore water composition, because the two settings are not strikingly different in terms of thermodynamic drive or water chemistry (White et al., 2001; White and Brantley, 2003).

### 5.2. Role of microbial activity

To better understand the role of microbial activity in promoting chemical weathering in the Middendorf, we recalculated the model

<sup>1</sup> The study cited reports reaction rates per unit surface area, the values of which are numerically equivalent to the intrinsic rate constant because  $1-Q/K$  for the conditions they consider is close to unity.

without altering the rate constants, assuming first an absence of microbial activity, and then setting activity to twice the rate of the original calculation (Fig. 8). In the simulation ignoring microbial activity, pH in the flowing groundwater rises rapidly, reaching a value of nearly 10 at the outlet. Weathering drives the groundwater alkaline because of the lack of acid production by the iron reducers, which contribute  $\text{CO}_2$ , and because carbonate from microbial respiration is not available to help buffer pH.

At high pH, the aluminosilicate and carbonate minerals are less undersaturated than in the original model, and hence dissolve more slowly, as shown for illite in Fig. 8. When the rate is doubled, in contrast, weathering proceeds at an accelerated rate. The pH remains more acidic than in the original model, and in response weathering proceeds more quickly. These results point to a direct relationship in which microbial activity within the aquifer promotes chemical weathering by generating  $\text{CO}_2$  as a source of acid, as well as producing dissolved carbonate, which buffers pH.

### 5.3. Source of acid

Fig. 9 shows the amount of acid as  $\text{CO}_2$  present in groundwater at recharge and the cumulative contribution of  $\text{CO}_2$  by microbial activity along the aquifer, together with the cumulative amount of acid consumed by weathering. The net acid content of the groundwater at any point in the aquifer is the sum of first two quantities, less the third. At recharge, Middendorff groundwater contains about 0.6 mM of  $\text{CO}_2$  (Table 1; Park et al., 2006), a value considerably in excess of 0.011 mM  $\text{CO}_2$  expected for water in equilibrium with the atmosphere. The additional  $\text{CO}_2$  was apparently derived from sources at the recharge point, such as root respiration and organic decay.

Along the non-marine sediments of the upper coastal plain, iron reducers in the simulation contribute a total of about 0.5 mM  $\text{CO}_2$  to the flowing groundwater. Sulfate reducers in the marine sediments of the lower coastal plain produce bicarbonate rather than  $\text{CO}_2$  and hence are not a source of acid. Slightly less than half of the acid contributed to Middendorff groundwater, then, is derived from microbial activity in the aquifer. The remainder is derived from the recharge area, although only about 1% of the total is of direct atmospheric origin, as  $\text{CO}_2$  dissolved in rainwater.

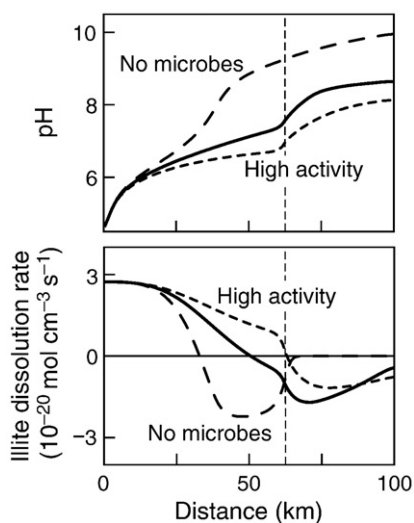


Fig. 8. Distribution of pH and the rate of illite reaction in a reactive transport model calculated assuming no microbial respiration occurs in the aquifer (broken line), and one in which the respiration rate is twice that assumed in the original model (fine broken line). Solid line shows results of the original calculation (Figs. 3, 5 and 6).

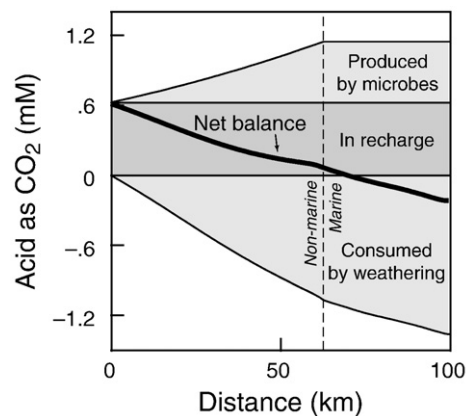


Fig. 9. Acid balance in the Middendorff aquifer. Acid is supplied as  $\text{CO}_2$  derived from the recharge area, and generated by iron reducing bacteria in the aquifer; it is consumed by weathering reactions. Bold line shows net acid content, the sum of the first two quantities, less the third.

### 5.4. Coexistence of iron and sulfate reduction

We repeated the calculation procedure to test whether the modeling can help resolve the question already discussed (Section 2.6) of whether in the upper coastal plain sulfate reducers are active along with iron reducers. In the recalculation, we eliminated the iron reducers in the upper coastal plain, replacing them with sulfate reducers as the source of inorganic carbonate. We were able to adequately fit the model results to the groundwater composition in the Middendorff by reducing the effective rate constant for albite in the simulation to 25%, and that for quartz to 17% of its original value. We were, therefore, unable to resolve this question with our reactive transport model.

## 6. Closing remarks

The reactive transport models in this study portray chemical weathering in the Middendorff aquifer as a slow process by which groundwater reacts gradually toward equilibrium with minerals in the aquifer. Reaction in the model proceeds slowly because the rate constants predicted are small, much smaller than those measured in the laboratory or inferred from weathering rates in soils; the rate constants are smaller even than expected by projecting the known decrease in their values with the duration of weathering to the geologic age of the Middendorff. The small rate constants probably reflect a marked decrease in the reactivity of the mineral surfaces as they have weathered over geologic time, coupled with a loss of contact area in the aquifer between groundwater and the mineral surfaces.

Weathering in the aquifer is largely a result of biological activity. About half the acid consumed by the weathering process is derived at the recharge area, by processes such as root respiration and organic decay, and about half from microbial activity in the aquifer. Atmospheric  $\text{CO}_2$  dissolved in rainwater accounts for only about 1% of the acid contributed to the groundwater.

### Acknowledgments

We thank two anonymous reviewers for their helpful comments. This work was supported by the Department of Energy under Grant DE-FG02-02ER15317. Any opinions, findings, and conclusions or recommendations expressed in this material are those of the authors and do not necessarily reflect those of the Department of Energy.

### Appendix A. Supplementary data

Supplementary data associated with this article can be found, in the online version, at doi:10.1016/j.chemgeo.2008.10.011.

## References

- Amundson, R., 2003. Soil formation. In: Drever, J.I. (Ed.), *Treatise on Geochemistry*, vol. 5. Elsevier Science, p. 626.
- Appelo, C.A.J., Postma, D., 1993. *Geochemistry, Groundwater and Pollution*. A.A. Balkema, Rotterdam, Netherlands. 536 pp.
- Aucott, W.R., Roy, N.J., 1986. Elected aquifer-test information for the coastal plain aquifers of South Carolina. *Water Resources Investigations WRI 86-4159*, U.S. Geol. Surv., Columbia, SC, United States.
- Aucott, W.R., Speiran, G.K., 1985. Ground-water flow in the coastal plain aquifers of South Carolina. *Ground Water* 23 (6), 736–745.
- Banks, D., Frengstad, B., 2006. Evolution of groundwater chemical composition by plagioclase hydrolysis in Norwegian anorthosites. *Geochimica et Cosmochimica Acta* 70 (6), 1337–1355.
- Bennett, P.C., Hiebert, F.K., Choi, W.J., 1996. Microbial colonization and weathering of silicates in a petroleum-contaminated groundwater. *Chemical Geology* 132, 45–53.
- Berger, G., Cadore, E., Schott, J., Dove, P.M., 1994. Dissolution rate of quartz in lead and sodium electrolyte solutions between 25 and 300 °C: effect of the nature of surface complexes and reaction affinity. *Geochimica et Cosmochimica Acta* 58 (2), 541–551.
- Berner, R.A., 2006. GEOCARBSULF: a combined model for Phanerozoic atmospheric O<sub>2</sub> and CO<sub>2</sub>. *Geochimica et Cosmochimica Acta* 70 (23), 5653–5664.
- Bethke, C.M., 2008. *Geochemical and Biogeochemical Reaction Modeling*. Cambridge University Press. 564 pp.
- Blum, A.E., Stillings, L.L., 1995. Feldspar dissolution kinetics. In: White, A.F., Brantley, S.L. (Eds.), *Chemical Weathering Rates of Silicate Minerals*, vol. 31. Mineralogical Society of America, pp. 291–351.
- Carroll-Webb, S.A., Walther, J.V., 1988. A surface complex reaction model for the pH-dependence of corundum and kaolinite dissolution rates. *Geochimica et Cosmochimica Acta* 52 (11), 2609–2623.
- Casey, W.H., Banfield, J.F., Westrich, H.R., McLaughlin, L., 1993. What do dissolution experiments tell us about natural weathering? *Chemical Geology* 105 (1–3), 1–15.
- Chapelle, F.H., Lovley, D.R., 1990. Rates of microbial metabolism in deep coastal plain aquifers. *Applied and Environmental Microbiology* 56 (6), 1865–1874.
- Chapelle, F.H., Lovley, D.R., 1992. Competitive exclusion of sulfate reduction by Fe(III)-reducing bacteria; a mechanism for producing discrete zones of high-iron ground water. *Ground Water* 30 (1), 29–36.
- Delany, J.M., Lundeen, S.R., 1990. The LLNL thermochemical database. Lawrence Livermore National Laboratory Report UCRL-21658. Lawrence Livermore National Laboratory.
- Drever, J.I., Hurcomb, D.R., 1986. Neutralization of atmospheric acidity by chemical weathering in an alpine drainage basin in the North Cascade Mountains. *Geology* 14 (3), 221–224.
- Fehrenbach, L., Maurette, M., Guichard, F., Havette, A., Monaco, A., 1983. Paleocorrosion studies in deep sea sediments and the geological disposal of nuclear wastes. *Journal of Non-Crystalline Solids* 67 (1–3), 287–303.
- Galloway, J.N., 1979. Alteration of trace metal geochemical cycles due to the marine discharge of wastewater. *Geochimica et Cosmochimica Acta* 43 (2), 207–218.
- Ganor, J., Lu, P., Zheng, Z., Zhu, C., 2007. Bridging the gap between laboratory measurements and field estimations of silicate weathering using simple calculations. *Environmental Geology* 53 (3), 599–610.
- Hereford, A., Keating, E., Guthrie, G., Zhu, C., 2007. Reactions and reaction rates in the regional aquifer beneath the Pajarito Plateau, north-central New Mexico, USA. *Environmental Geology* 52 (5), 965–977.
- Hiebert, F.K., Bennett, P.C., 1992. Microbial control of silicate weathering in organic-rich ground water. *Science* 258 (5080), 278–281.
- Kenoyer, C.J., Bowser, C.J., 1992. Groundwater chemical evolution in a sandy silicate aquifer in northern Wisconsin 2. Reaction modeling. *Water Resources Research* 28 (2), 591–600.
- Lasaga, A.C., Soler, J.M., Ganor, J., Burch, T.E., Nagy, K.L., 1994. Chemical weathering rate laws and global geochemical cycles. *Geochimica et Cosmochimica Acta* 58 (10), 2361–2386.
- Lee, R.W., Strickland, D.J., 1988. Geochemistry of groundwater in Tertiary and Cretaceous sediments of the southeastern coastal plain in eastern Georgia, South Carolina, and southeastern North Carolina. *Water Resources Research* 24 (2), 291–303.
- Lovley, D.R., Goodwin, S., 1988. Hydrogen concentrations as an indicator of the predominant terminal electron-accepting reactions in aquatic sediments. *Geochimica et Cosmochimica Acta* 52 (12), 2993–3003.
- McMahon, P.B., Chapelle, F.H., 1991. Microbial production of organic acids in aquitard sediments and its role in aquifer geochemistry. *Nature (London)* 349 (6306), 233–235.
- Murphy, E.M., Schramke, J.A., 1998. Estimation of microbial respiration rates in groundwater by geochemical modeling constrained with stable isotopes. *Geochimica et Cosmochimica Acta* 62 (21–22), 3395–3406.
- Nugent, M.A., Brantley, S.L., Pantano, C.G., Maurice, P.A., 1998. The influence of natural mineral coatings on feldspar weathering. *Nature* 395 (6702), 588–591.
- Park, J., Sanford, R.A., Bethke, C.M., 2006. Geochemical and microbiological zonation of the Middendorf aquifer, South Carolina. *Chemical Geology* 230 (1–2), 88–104.
- Parkhurst, D.L., Plummer, L.N., Thorstenson, D.C., 1982. BALANCE — a computer program for calculating mass transfer for geochemical reactions in groundwater. *Water Resources Investigations WRI 82-14*. U. S. Geological Survey, Reston, VA.
- Plummer, L.N., Prestemon, E.C., Parkhurst, D.L., 1994. An interactive code (Netpath) for modeling net geochemical reactions along a flow path. *Water Resources Investigation WRI 94-4169*. U.S. Geological Survey, Reston, Virginia.
- Rademacher, L.K., Clark, J.F., Hudson, G.B., Erman, D.C., Erman, N.A., 2001. Chemical evolution of shallow groundwater as recorded by springs, Sagehen basin; Nevada County, California. *Chemical Geology* 179 (1–4), 37–51.
- Reid, M.S., Renken, R.A., Wait, R.S., Aucott, W.R., Lee, R.W., 1986. Hydrologic and geologic analysis of two wells in Marion County, South Carolina. *Water Resources Investigation 86-4102*. U.S. Geological Survey, Reston, VA.
- Roberts, J.A., et al., 2004. Microbial precipitation of dolomite in methanogenic groundwater. *Geology* 32 (4), 277–280.
- Royer, D.L., 2006. CO<sub>2</sub>-forced climate thresholds during the Phanerozoic. *Geochimica et Cosmochimica Acta* 70 (23), 5665–5675.
- Sargent, K.A., Fliermans, C.B., 1989. Geology and hydrology of the deep subsurface microbiology sampling sites at the Savannah River Plant, South Carolina. *Geomicrobiology Journal* 7 (1), 3–13.
- Schulz, M.S., White, A.F., 1999. Chemical weathering in a tropical watershed, Luquillo Mountains, Puerto Rico III: quartz dissolution rates. *Geochimica et Cosmochimica Acta* 63 (3–4), 337–350.
- Soler, J.M., Lasaga, A.C., 1998. An advection–dispersion–reaction model of bauxite formation. *Journal of Hydrology* 209 (1–4), 311–330.
- Speiran, G.K., Aucott, W.R., 1994. Effects of sediment depositional environment and ground-water flow on the quality and geochemistry of water in aquifers in sediments of Cretaceous age in the coastal plain of South Carolina. *Water Supply Paper 2416*, U. S. Geological Survey.
- Velbel, M.A., 1993. Constancy of silicate–mineral weathering–rate ratios between natural and experimental weathering: implications for hydrologic control of differences in absolute rates. *Chemical Geology* 105 (1–3), 89–99.
- Volk, T., 1987. Feedbacks between weathering and atmospheric CO<sub>2</sub> over the last 100 million years. *American Journal of Science* 287, 763–779.
- Welch, S.A., Ullman, W.J., 1999. The effect of microbial glucose metabolism on bytownite feldspar dissolution rates between 5° and 35 °C. *Geochimica et Cosmochimica Acta* 63 (19–20), 3247–3259.
- White, A.F., 2003. Natural weathering rates of silicate minerals. In: Drever, J.I. (Ed.), *Treatise on Geochemistry. Surface and Ground Water, Weathering, and Soils*, vol. 5. Elsevier, New York, pp. 133–168.
- White, A.F., et al., 1996. Chemical weathering rates of a soil chronosequence on granitic alluvium: I. Quantification of mineralogical and surface area changes and calculation of primary silicate reaction rates. *Geochimica et Cosmochimica Acta* 60 (14), 2533–2550.
- White, A.F., Brantley, S.L., 2003. The effect of time on the weathering of silicate minerals: why do weathering rates differ in the laboratory and field? *Chemical Geology* 202 (3–4), 479–506.
- White, A.F., et al., 2001. Differential rates of feldspar weathering in granitic regoliths. *Geochimica et Cosmochimica Acta* 65 (6), 847–869.
- Xu, T., Apps, J.A., Pruess, K., 2005. Mineral sequestration of carbon dioxide in a sandstone–shale system. *Chemical Geology* 217 (3–4), 295–318.
- Zhu, C., 2005. In situ feldspar dissolution rates in an aquifer. *Geochimica et Cosmochimica Acta* 69 (6), 1435–1453.